Sensor applications

# Light-Controlled Thin Film Backscatter Device Using Additive Manufacturing

Boxuan Xie*, Lauri Mela, Jari Lietzén, Kalle Ruttik**, Alexis Dowhuszko***, and Riku Jäntti***

*Department of Information and Communications Engineering, Aalto University, 02150 Espoo, Finland*
**Graduate Student Member, IEEE*
***Member, IEEE*
****Senior Member, IEEE*

Manuscript received 4 March 2024; revised 31 March 2024; accepted 18 April 2024. Date of publication 30 April 2024; date of current version 9 May 2024.

Abstract—The recent demand for flexible printed electronics integration technologies in, e.g., additively manufactured radio frequency (RF) components and modules for Internet of Things (IoT) gains growing popularity. Inkjet printing on flexible substrates is one of the most preferable techniques because of easy fabrication and compact packaging. This letter presents a compact thin film backscatter device (BD) designed for visible light communication (VLC)-enabled IoT scenarios. The BD converts light carrying sensor data into RF signals, transmitting them at the 2.4 GHz band by employing ambient backscatter communication. The integration of inkjet-printed circuitry, antenna, and lumped components on polyethylene terephthalate substrates through additive manufacturing highlights advancement in device compactness and flexibility. Experiment results validate the BD's robust performance under various lighting conditions for data transmission, showing potential for facilitating VLC-IoT applications.

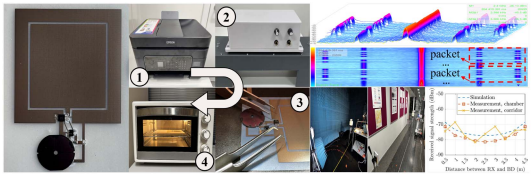


Index Terms—Sensor applications, additive manufacturing, backscatter communication, Internet of Things (IoT), printed electronics, visible light communication (VLC).

## I. INTRODUCTION

The ubiquitous presence of configurable lighting, such as light-emitting diodes (LEDs), support sensors to transmit their data through optical wireless channels, known as visible light communication (VLC)-enabled Internet of Things (IoT) [1]. VLC offers a promising alternative to conventional wireless sensor networks in IoT applications because of its unique advantages. VLC utilizes the existing lighting infrastructure, making it a cost-effective solution that avoids the use of crowded radio frequency (RF) spectrum. This alleviation of spectrum congestion is crucial as the number of sensors and IoT devices is expected to be continuously growing. In this scenario, data from sensors are embedded in light signals used for VLC cooperating with IoT infrastructures.

Available VLC-enabled IoT schemes involve complex scattering and reception mechanisms and circuitry for relaying and receiving light signals from sensors [2]. For instance, they adopt optical relay nodes, such as retroreflectors, and optical readers, such as photodetectors, for exchanging data from sensors. However, such components are absent from most existing IoT front-ends. Alternatively, the light signals can be converted into RF signals that can then be detected with conventional RF receivers by adopting a transponder device. To transmit the RF signals in very high-frequency (VHF) band and beyond, typical transponders consist of expensive energy-hungry components, such as carrier synthesizers and power amplifiers. Ambient backscatter communication (AmBC) [3], [4] addresses this challenge by employing ambient RF signals, such as WiFi and TV, enabling a self-powered backscatter device (BD) to transmit data by modulating and reflecting ambient RF signals. Hence, we propose a combination of VLC and AmBC shown in Fig. 1(a). In this scenario, the data originating from sensors and sent using VLC are converted to electrical signals at a BD, and the BD then transmits the data by modulating and reflecting ambient RF signals. This leads to a notable reduction in energy consumption.

In addition, the fusion of advanced device packaging and integration technologies enabled by the additive manufacturing of RF components with low-cost inkjet printing method is considered for the fabrication of flexible BDs and sensors [5], [6], [7]. This letter proposes a compact thin-film BD that receives sensor data from LEDs and transmits them to RF receivers at the 2.4 GHz industrial, scientific, and medical (ISM) band, as shown in Fig. 1(b). Benefiting from additive manufacturing methods with commercial off-the-shelf materials, we integrate the inkjet-printed circuit board, antenna, and lumped components on flexible polyethylene terephthalate (PET) substrates for realizing the device functionalities, including light harvest, RF modulation, and reflection.

## II. DESIGN

The design of BD is shown in Fig. 1(c) with circuit diagram (left) and manufacturing footprints (right), comprising lumped elements mounted on a thin-film inkjet-printed circuit board and an inkjet-printed coplanar waveguide (CPW) antenna. A solar cell (SC) BCSC241D4 harvests modulated light from the sensors and converts the light into the voltaic signal denoted by $V_{sc}$. The $V_{sc}$ feeds the positive input of a comparator (CMP) TLV7031 and an $RC$ low-pass filter (LPF) composed by a 100 kΩ resistor (R1) and a 0.1 $\mu$F capacitor (C1), respectively. This LPF has a cutoff frequency of 15 Hz at 3 dB, and outputs the dc component of $V_{sc}$, denoted by $V_{LPF}$ for feeding the negative input of the CMP. Hence, the CMP compares the ac and dc components of $V_{sc}$, setting the output voltage $V_{CTRL}$ to high($V_H$), if $V_{sc} > V_{LPF}$, otherwise setting $V_{CTRL}$ to low ($V_L$). The output signal $V_{CTRL}$

Corresponding author: Boxuan Xie (e-mail: boxuan.xie@aalto.fi).
Associate Editor: Ravinder Dahiya.
Digital Object Identifier 10.1109/LSENS.2024.3395450

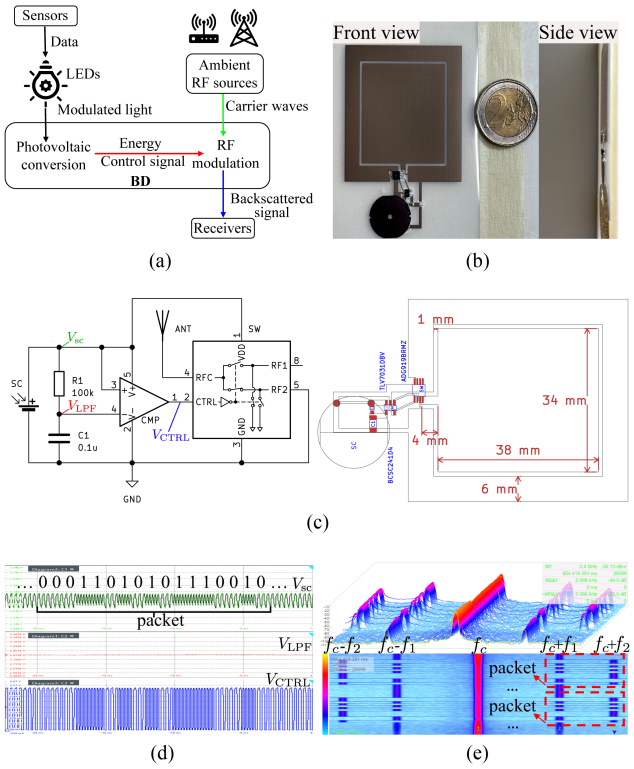


Fig. 1. BD. (a) Combination of VLC and AmBC. (b) Prototype after additive manufacturing. (c) Schematic and footprint layout. (d) Circuit outputs example. (e) Received signals in OTA demonstration.

is then used for controlling an RF switch ADG919 for backscatter modulation and reflection. For visualizing circuit operations, three probes of an oscilloscope are placed in the circuit shown in Fig. 1(c), monitoring signals $V_{sc}$, $V_{LPF}$, and $V_{CTRL}$. The recorded signals are shown in Fig. 1(d) as an example, where the light is modulated with binary frequency shift keying (2FSK) baseband signal. The RF switch is connected to a CPW antenna, switching the termination of antenna between two loads $Z_i \in \{Z_1, Z_2\}$. Assuming that the antenna is matched to characteristic impedance $Z_a$, the complex reflection coefficient [8] is expressed by $\Gamma_i = (Z_i - Z_a^*)/(Z_i + Z_a)$, where $^*$ denotes the complex conjugation. The corresponding modulation factor $M$ [8] is then $M = \frac{1}{4}|\Gamma_1 - \Gamma_2|^2$. The modulator achieves the maximum of $M = 1$, when $Z_1 = \infty$ and $Z_2 = 0$, corresponding to the switch either opening or shorting the antenna termination. The signal $V_{CTRL}$ controls the RF switch, and is converted from the modulated light carrying sensor data. Here, the 2FSK baseband signal is implemented for demonstrating sensor data transmission, such that the switching speed varies between predefined frequencies $f_1$ and $f_2$. When the ambient RF signal with a carrier frequency of $f_c$ arrives at the antenna, it gets mixed with the switch control signal $V_{CTRL}$ by the switching operation. The modulated backscatter signals with frequencies $f_c \pm f_1$ and $f_c \pm f_2$ will reflect and carry the sensor data. The reader detects and demodulates the backscattered signal and recovers the sensor data.

As a key component of the BD, the integrated CPW antenna affects ambient RF signal harvest and backscatter signal radiation at the aimed frequency band. Hence, the antenna is first designed and characterized separately from the device circuit. The measured return loss is 29.4 dB at 2.45 GHz with a 10-dB bandwidth of 575 MHz. The maximum realized gain is 1.9 dBi with a half power beamwidth around 99° at 2.42 GHz. The details of original antenna design can be found in our previous study [9].

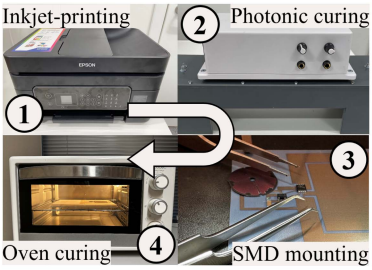


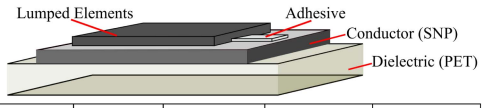


| Layer | Thickness | Permittivity | Loss tangent | Conductivity |
|---|---|---|---|---|
| Conductor (SNP) | 440 nm | -- | -- | $6\times10^6$ S/m |
| Dielectric (PET) | 135 μm | 4.8 | 0.138 | -- |

(b)

Fig. 2. Additive manufacturing. (a) Process. (b) Materials after curing.

As a demonstration of over-the-air communication, a sensor node emulated by a Raspberry Pi Pico provided its 17-bit data packet "00011010101110010" with 2FSK-modulated square wave to an LED array with $f_1 = 3$ kHz representing "0" and $f_2 = 5$ kHz representing "1". The modulated light was then received by the BD, converted to the switch control signal $V_{CTRL}$, and modulated with a 2.4 GHz continuous wave carrier signal. The spectrum and spectrogram of reader-received signals were shown in Fig. 1(e), where the original data from the sensor node have been recovered.

## III. ADDITIVE MANUFACTURING

An additive manufacturing method with commercial off-the-shelf materials is adopted to integrate the BD circuitry and antenna on a flexible thin-film substrate for making the device compact (W48 mm × L70 mm × H1 mm) and lightweight (0.9 g). The manufacturing process shown in Fig. 2(a) includes: (1) inkjet printing of circuit board and antenna; (2) curing the ink on the printed sheet; (3) mounting surface-mounted device (SMD) components on the printed footprints with conductive adhesive; and (4) curing the adhesive. The structure and parameters of used materials are shown in Fig. 2(b).

Silver nanoparticle (SNP) ink NBSIJ-MU01 is used to print the conductive layer of the design on an A4-size PET substrate NB-TP-3GU100 (microporous $Al_2O_3 - PVA$ single-sided coating) used with a low-cost inkjet printer Epson WF-2840 DWF (resolution 5760 × 1440 DPI). The microporous coating on the substrate facilitates the efficient absorption and swift reaction of the SNP ink, leading to the formation of highly conductive layers. After the inkjet printing, the printed surface undergoes a photonic curing treatment using a 1500-W Xenon flash tube XOP-15 (wavelength 200–1000 nm) for 15 s to cure the ink efficiently. The photonic curing can mitigate thermal stress on the substrate. This reduction in thermal stress minimizes warping, degradation, and curing time, offering a distinct advantage over traditional convective oven curing methods that require high temperatures.

Then, SMD components are mounted to their footprints on the printed circuit board by using conductive epoxy adhesive MG Chemicals 9410 and thin tweezers. Finally, for curing adhesive, the entire device is cured in an oven with 90 °C for 1 h. The completed device is shown in Fig. 1(b).

Table 1. Measurement Setup

| Illumination intensity response | | Modulated light frequency response | |
|---|---|---|---|
| Light sources | Ambient light intensity | Light sources | Ambient light intensity |
| LED | – | LED | – |
| LED + Ambient-1 | 246 lx | LED + Ambient-1 | 246 lx |
| LED + Ambient-2 | 500 lx | LED + Ambient-1 + Ambient-2 | 746 lx |

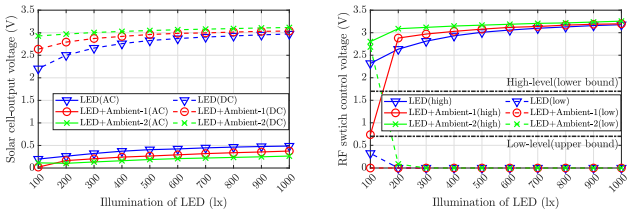


(a) (b)

Fig. 3. Illumination intensity response of (a) $V_{sc}$ and (b) $V_{CTRL}$.

## IV. EXPERIMENTS AND EVALUATION

### A. Illumination Intensity Response

The BD utilizes intensity-modulated light as its energy source and as the sensor data carrying signal. Maintaining a sufficient light intensity is critical to ensure that the modulated light can support both functions. First, a certain level of average light intensity is required to produce the operating current of the circuitry. Second, the amplitude of the electrical signal at the output of the solar cell has to reach a level that can drive the comparator to change its output state. Hence, the functioning of the BD is evaluated with various intensities of modulated light with different amounts of ambient, unmodulated illumination listed in Table 1.

An adjustable, constant current LED driver with a modulation input is driven by a function generator using a 3-kHz square wave signal emulating sensors baseband signal. An array of seven phosphor-converted white LEDs (OSRAM 7 GW J9LHS2.4 M, 3500 K) is used as the modulated light source. The emitted white light contains multiple wavelengths (400–800 nm) within the visible light spectrum. Modulated light intensities 100–1000 lx at the BD are tested while monitoring the output of the solar cell $V_{sc}$, the low-pass filtered signal $V_{LPF}$, and the comparator output $V_{CTRL}$. It should be noted that all light intensities reported in this letter are measured with an illuminance meter collocated with the solar cell of BD. Testing is repeated with two different ambient light sources present, a fluorescent office light (Ambient-1) and another identical, unmodulated LED array (Ambient-2) with light intensities of 246 and 500 lx at the BD, respectively. The objective is to find possible lower and upper bounds for modulated light intensity within the range of levels acceptable for indoor lighting. The ambient light sources are introduced to study whether they have an impact on the functioning of the circuitry.

Fig. 3(a) shows the dc level and ac amplitude of the solar cell output $V_{sc}$. The RF switch and comparator require minimum supply voltages of 1.65 and 1.6 V, respectively. Therefore, the required dc level is 1.65 V plus half of the ac amplitude to ensure that the instantaneous voltage keeps within the operating range. It is clear that the dc level is suitably high at all tested illumination levels with or without added ambient light. However, there is a trend of decreasing dc level when the light intensity is decreased pointing toward a threshold level somewhere below 100 lx. In terms of the achieved dc level, the addition of ambient light contributes to a better performance, which is expected as the total light intensity is increased. A similar trend is seen with the ac amplitude decreasing in response to the lower intensity of the modulated light. However, the addition of ambient light has the opposite effect on ac amplitude compared to the effect on the dc level. This indicates that ambient light can impact the proper functioning of the BD depending on the ratios of the modulated light and the ambient light intensities. Fig. 3(b) shows the high and low voltage levels of the comparator output being the RF switch control signal $V_{CTRL}$. The threshold voltages for those are the logic high (lower bound 1.7 V) and low (upper bound 0.7 V) levels for controlling the switch. The result indicates that in the range of modulated light intensity from 200 to 1000 lx, the circuit can successfully control the switch for modulation, with or without additional ambient light. At 100 lx, the operation is marginal when only modulated light is present and fails with the addition of the ambient lights. Such illumination requirements can be fulfilled in most indoor spaces [10].

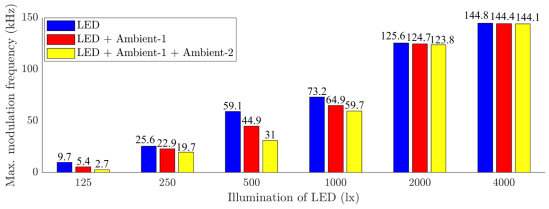


Fig. 4. Modulated light frequency response of the BD.

### B. Modulated Light Frequency Response

The modulation rate contributes to the achievable data rate of backscatter communications. Due to the low-pass characteristic of the solar cell [11], the available ac amplitude of $V_{sc}$ decreases with higher modulation rates. As seen from results in Section IV-A, the ac amplitude is also affected by the modulated light intensity. Hence, it is relevant to study the limits of the modulation rate in varying conditions of illumination. The measurement setup is otherwise the same as in Section IV-A, but the range of modulated light intensity is from 125 to 4000 lx. The modulation rate is varied instead of being fixed. The higher intensities in this experiment are reached by moving the LEDs closer to the BD. Moreover, the ambient lights, if any, are configured to produce illuminations of 246 and 746 lx by having the fluorescent office light (Ambient-1) always active.

The modulation rate in each scenario is varied while monitoring the output of the comparator. The thresholds are found at rates where the comparator output is still correct, i.e., switching at the modulation rate with clean transitions without oscillations. It is important to note that the modulated light output from the LED array using the driver has been verified with an amplified photodetector Thorlabs PDAPC2. The LED and driver combination can reach rates in excess of 200 kHz with the limitation being in the driver chip OnSemi CAT4109.

The results from this experiment are illustrated in Fig. 4, where a clear trend of increasing modulation rates with increasing modulated light intensities is seen. The additional ambient light has a negative influence on the achievable modulation rate as would be expected from the results in Section IV-A. The only exception is at 2000 and 4000 lx levels where the modulated light overpowers the ambient lights and the modulation rate is only marginally affected. The result indicates that there seems not to be any negative effect on performance with increasing intensities, i.e., the solar cell does not saturate in any way, at least within the range of intensities tested. In practice, higher illumination intensities may be impractical for the BD intended for use in environments with standard indoor lighting levels [10]. At lighting levels of 250–500 lx, modulation rates of approximately 20–60 kHz can be reached, depending on the presence of ambient

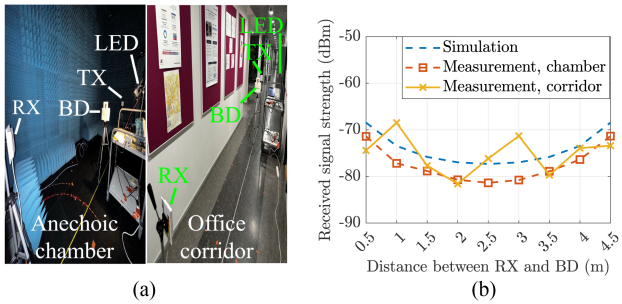


(a) (b)

Fig. 5. OTA measurement. (a) Setup. (b) Received signal strength.

light sources. With increasing ratio of modulated light intensity to ambient light intensity, the performance degradation is reduced. The BD demonstrates a moderate tolerance to ambient light, maintaining usable modulation rates even when the ratios fall below one.

### C. Over-the-Air Backscatter Propagation

The fabricated BD is also validated with an OTA bistatic dislocated backscatter radio setup in both an anechoic chamber without ambient light and an office corridor with various ambient light illumination from 60 to 150 lx at the BD, shown in Fig. 5(a). The backscatter radio setup is composed of an ambient RF emitter (TX), the sensor node Raspberry Pi Pico connected to the LED module, the BD, and a spectrum analyzer as a receiver (RX). The sensor node sends its data to the LED module with 2FSK baseband signal, working in the same manner discussed in Section II. The BD is moved between the TX and RX with a 5.0 m distance in 0.5 m steps and is illuminated by the LED array with a fixed illumination intensity of 100 lx. The received backscatter signal strength is recorded by the spectrum analyzer at all BD's locations, shown in Fig. 5(b). For comparing measurement results with the well-known backscatter radio propagation model [8], simulations are also implemented with the realistic parameters used by measurement configurations. The propagation model for the bistatic dislocated scheme is expressed by

$$P_{\mathrm{R}} = \frac{P_{\mathrm{T}} G_{\mathrm{T}} G_{\mathrm{R}} G_{\mathrm{BD}}^2 \lambda^4 X_{\mathrm{f}} X_{\mathrm{b}} M}{(4\pi)^4 r_{\mathrm{f}}^2 r_{\mathrm{b}}^2 \Theta^2 B_{\mathrm{f}} B_{\mathrm{b}} L_{\mathrm{BDBC}}} \tag{1}$$

where $P_{\mathrm{R}}$ denotes the RX received backscatter signal power, and $P_{\mathrm{T}}$ (10 dBm) denotes ambient source emitted signal power. $G_{\mathrm{T}}$ (6.5 dBi), $G_{\mathrm{R}}$ (6.5 dBi), and $G_{\mathrm{BD}}$ (1.8 dB) are measured gains at the ambient source, RX, and BD, respectively. $\lambda$ (0.125 m) is the wavelength. $\Theta$ (0 dB) implies the on-object gain penalty of the BD. $X_{\mathrm{f}}$ (0 dB) and $X_{\mathrm{b}}$ (0 dB) denote the polarization mismatch of forward link (from the emitter to BD) and backscatter link (from the BD to RX), respectively. $M$ (0.48) is the modulation factor of the RF switch at 2.4 GHz measured using a vector network analyzer. $r_{\mathrm{f}}$ and $r_{\mathrm{b}}$ are the distances of the forward and backscatter links, respectively. $B_{\mathrm{f}}$ (0 dB) and $B_{\mathrm{b}}$ (0 dB) are the path-blockage loss of the forward and backscatter link, respectively. $L_{\mathrm{BDBC}}$ (4.4 dB) is the measured cabling loss. The root-mean-square error between model-predicted strength and measured signal strength is 3.4 dB in the anechoic chamber and 4.2 dB in the corridor. More fluctuation in signal strength was observed in the corridor measurement due to reflection and diffraction.

## V. CONCLUSION

This letter presented a compact thin-film BD that receives sensor data from LEDs and transmits the data to RF receivers at the 2.4 GHz ISM band. The BD was manufactured by additive methodology, including inkjet printing, surface mounting, and photonic- and oven-curing. The BD responses to various modulated light illumination from 100 to 1000 lx have been evaluated with and without ambient lighting interference, indicating that the device is suitable for most of indoor lighting conditions. The BD frequency response to LEDs has also been evaluated, showing that a maximum backscatter modulation rate of 144.8 kHz can be achieved. The over-the-air end-to-end sensor data transmission has been demonstrated in an anechoic chamber and office corridor and has been validated with the propagation model. Results indicated that the manufactured BD has potential to facilitate the combination of VLC and IoT.

## ACKNOWLEDGMENT

This work was supported by the Academy of Finland under Grant 334197 and Grant 352912. The authors appreciate Alp Karakoç, Kalle Koskinen, and Juho Kerminen for discussion.

## REFERENCES

[1] I. Demirkol, D. Camps-Mur, J. Paradells, M. Combalia, W. Popoola, and H. Haas, "Powering the Internet of Things through light communication," *IEEE Commun. Mag.*, vol. 57, no. 6, pp. 107–113, Jun. 2019.

[2] M. H. Ullah, G. Gelli, and F. Verde, "Visible light backscattering with applications to the Internet of Things: State-of-the-art, challenges, and opportunities," *Internet Things*, vol. 22, 2023, Art. no. 100768.

[3] R. Duan, X. Wang, H. Yiğitler, M. U. Sheikh, R. Jäntti, and Z. Han, "Ambient backscatter communications for future ultra-low-power machine type communications: Challenges, solutions, opportunities, and future research trends," *IEEE Commun. Mag.*, vol. 58, no. 2, pp. 42–47, Feb. 2020.

[4] V. Liu, A. Parks, V. Talla, S. Gollakota, D. Wetherall, and J. R. Smith, "Ambient backscatter: Wireless communication out of thin air," *ACM Comput. Commun. Rev.*, vol. 43, no. 4, pp. 39–50, 2013.

[5] C. Song et al., "Advances in wirelessly powered backscatter communications: From antenna/RF circuitry design to printed flexible electronics," *Proc. IEEE*, vol. 110, no. 1, pp. 171–192, Jan. 2022.

[6] J. Wiklund et al., "A review on printed electronics: Fabrication methods, inks, substrates, applications and environmental impacts," *J. Manuf. Mater.*, vol. 5, no. 3, 2021, Art. no. 89.

[7] S. Khan, L. Lorenzelli, and R. S. Dahiya, "Technologies for printing sensors and electronics over large flexible substrates: A review," *IEEE Sens. J.*, vol. 15, no. 6, pp. 3164–3185, Jun. 2015.

[8] J. D. Griffin and G. D. Durgin, "Complete link budgets for backscatter-radio and RFID systems," *IEEE Antennas Propag. Mag.*, vol. 51, no. 2, pp. 11–25, Apr. 2009.

[9] J. Kerminen, B. Xie, L. Mela, A. Karakoç, K. Ruttik, and R. Jäntti, "Low-cost thin film patch antennas and antenna arrays with various background wall materials for indoor wireless communications," *Flex. Print. Electron.*, vol. 8, no. 2, 2023, Art. no. 025013.

[10] "Indoor lighting in the public and private service sectors guidelines." Accessed: Mar. 3, 2024. [Online]. Available: https://ec.europa.eu/research/participants/documents/downloadPublic?documentIds=080166e5b6d1bf85&appId=PPGMS

[11] S. Das, E. Poves, J. Fakidis, A. Sparks, S. Videv, and H. Haas, "Towards energy neutral wireless communications: Photovoltaic cells to connect remote areas," *Energies*, vol. 12, no. 19, 2019, Art. no. 3772.